Journal of Wood Science (2018) 64:347–355
https://doi.org/10.1007/s10086-018-1718-8

ORIGINAL ARTICLE

Determination of physical and chemical properties and degradation of archeological Japanese cypress wood from the Tohyamago area using near-infrared spectroscopy

Tetsuya Inagaki[1] · Hitoshi Yonenobu[2] · Yuuki Asanuma[1] · Satoru Tsuchikawa[1]

Received: 26 December 2017 / Accepted: 20 February 2018 / Published online: 6 April 2018

Abstract
Here, we evaluated the application of near-infrared (NIR) spectroscopy for estimating the degradation level of archeological wood samples from the Tohyamago area, the dendrochronological ages of which were also determined. The wood samples were radially cut from three logs obtained from the Tohyamago area. NIR reflectance spectra were measured from the tangential faces of air- and oven-dried wood samples using a Fourier transform NIR spectrophotometer. The second derivative spectra within the wavenumber range of 6400–5200 cm^{-1}, in which the effect of moisture content in wood is suspected to be insignificant, showed a characteristic behavior with age. By comparing the second derivative spectral change in our wood samples with that in wood degraded by aging, thermal treatment, fungal attack, and lightning reported in the literature, we found that the second derivative spectra of wood samples from one log was similar to those of wood degraded by hygrothermal treatment, whereas those of wood samples from another log was similar to those of wood degraded by brown-rot fungi. The physical and chemical properties of archeological wood were well predicted using a combination of partial least square regression analysis and NIR spectroscopy.

Keywords NIR spectroscopy · Archaeological wood · PLS regression analysis

Introduction

The study of wood aging is of great importance in Japan because of its long history of wood culture. Archeological wood decomposes at an archeological site because of natural phenomena, such as biodegradation, weathering (lightning), and aging [1]. Changes in archeological wood are evident through changes in the structure and physical, chemical, and mechanical properties of wood; however, the mechanism and rate of degradation of wood components significantly depend on environmental factors. For example, in waterlogged archeological wood samples, the most important effect of decay on chemical properties may manifest as compositional change within cell walls due to hydrolysis processes that mainly involve carbohydrate compounds, with a consequent increase in the relative lignin concentration [2–4]. The life span of Japanese cypress (*Chamaecyparis obtusa*) wood, which is used in construction, can exceed thousands of years when unexposed to biodegradation and weathering. Factors associated with wood aging during long-term use include combined effects of thermal oxidation by air oxygen and acid hydrolysis by adsorbed/bounded water and acids contained in wood.

Rapid and accurate estimation of the degradation level of archeological wood is important as it influences the selection of optimal restoration and conservation procedures. Near-infrared (NIR) spectroscopy is one of the best methods for this as it is rapid, inexpensive, nondestructive, and precise for evaluating molecular vibrations. The application of NIR spectroscopy in the evaluation of degradation level of wood due to aging [2–9], fungal decay [10–15], thermal treatment [16–19], and lightning [20, 21] has revealed that NIR spectroscopy is a promising method for monitoring chemical changes in degraded wood. Yonenobu et al. reported that compared with modern wood, the difference in the second derivative NIR spectra in archeological wood used for 1300 years under

✉ Satoru Tsuchikawa
st3842@agr.nagoya-u.ac.jp

[1] Graduate School of Bioagricultural Sciences, Nagoya University, Furo-cho, Chikusa-ku, Nagoya 464-8601, Japan

[2] Naruto University of Education, 748, Nakashima, Takashima, Naruto-cho, Naruto 772-8502, Japan

atmospheric conditions suggests that in archeological wood, hemicellulose and holocellulose is less, whereas lignin is more [5]. They also investigated the aging-associated changes in the fine structure of microfibrils in the cell wall using the deuterium exchange method [7]. Pecoraro et al. used NIR spectroscopy for evaluating the residual chemical composition of wood decayed by biotic agents when preserved for a long time in waterlogged conditions [4]. They established a highly reliable prediction model to assess the residual chemical composition of waterlogged archeological wood. Thus, the NIR second derivative spectral change is sensitive for detecting changes in the chemical structure of degraded wood.

Because the construction of a calibration model requires considerable amount of data, NIR spectroscopy is not widely used in archeological wood science in which only small number of archeological wood samples can be used. Therefore, we focused on wood samples that have been buried for a long time in the Tohyamago area. The degradation processes in archeological wood can be classified as follows: thermal oxidation, acid hydrolysis, weathering (lightening), and biodegradation [1]. Although thermal oxidation and acid hydrolysis are considered as dominant degradation processes in archeological wood samples from temples or statues [22], all the aforementioned processes are responsible for the degradation of buried wood samples. The advantage of using buried wood samples is the possibility of using many samples, thus enabling estimation of the sample's dendrochronological age. Recently, we selectively assessed the thermal and hygro-thermal treatment times of duplex heat-treated samples from the softwood hinoki cypress (*Chamaecyparis obtusa*) and the hardwood Japanese zelkova (*Zelkova serrata*) by NIR spectroscopy with principal component analysis (PCA) and spectral-kinetic analysis. In the study, wood samples from each species were thermally or hygro-thermally treated at 120, 130, 150, and 180 °C, and the second derivative spectra of these samples in the 6300–5450 cm^{-1} range, where moisture content has the smallest effect, were then subjected to PCA. It is shown that calculation of the inner product between the second derivative spectra of duplex heat-treated wood and a loading vector that explained the spectral variation due to thermal or hygro-thermal treatment allowed us to selectively assess the thermal and hygro-thermal treatment times [23].

In the present study, we evaluated the degradation level of archeological wood samples, the dendrochronological ages of which were also determined, using NIR spectroscopy. We compared the second derivative spectra of archeological wood with those of various other degraded wood samples reported in the literature for analyzing degradation history. We observed that the second derivative spectral change at the wavenumber range of 6400–5200 cm^{-1} highly depends on the type of degradation. Furthermore, partial least square (PLS) regression analysis was employed to predict various wood properties from NIR spectra.

Materials and methods

Samples

We collected two buried logs of Japanese cypress (NNTY99p and NNTY59a) (See Fig. 1a, b). One modern log of the same species was used for comparison. The former ones were found as fully buried tree stems, and were recovered from a single fluvial sediment layer at a recent renovation of river banks along the River Tohyama, Nagano Prefecture, Central Japan (N35°20′ E137°57′). The area of sampling is situated in a typical collapse terrain, and ancient imperial documents (e.g., *Shoku-Nihongi* in the eighth century) described that a big earthquake in AD 704 or 705 caused large-scale landslides and damming of the river, geomorphologically suggesting that the logs were all deposited simultaneously. The logs were wet when excavated, lacking most part of sapwood, but having color and scent specific of hinoki heartwood. No insect galleries were found under naked-eye and microscopic observation. It is, therefore, very likely that the buried logs had been to some extent kept in a uniform condition.

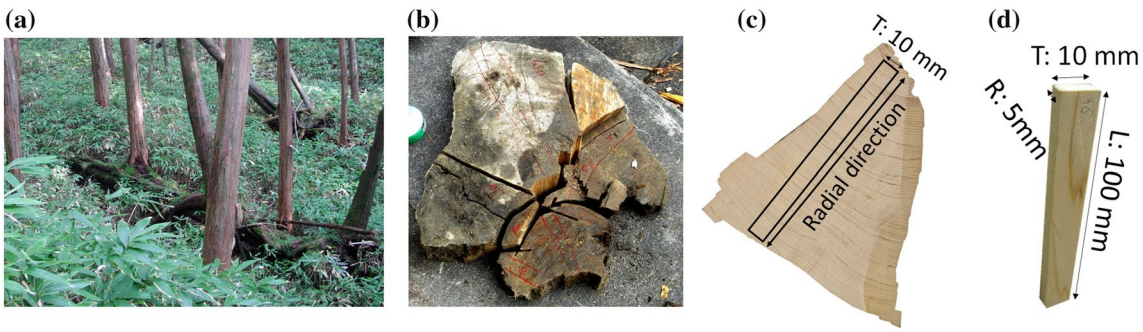

Fig. 1 Sample preparation

To obtain objective evidence for the ages, tree-ring dates, i.e., the years of outer-most ring formation, were determined by means of the standard dendrochronological method [24]. The buried and modern wood samples were successfully crossdated with the reference chronologies [25, 26], showing that the tree-ring dates were AD 623, 683, and 2001 for NNTY99p, NNTY59a and Modern, respectively.

A total of 121 experimental specimens were prepared from the samples (68, 27, and 26 for NNTY99p, NNTY59a, and Modern, respectively). The wood samples were radially cut to obtain a tangential dimension of 10 mm (Fig. 1c). The specimens were then cut tangentially to obtain dimensions of $5 \times 10 \times 100$ mm^3 (radial × tangential × longitudinal) (Fig. 1d). Each specimen contained 1–20 tree rings. The specimens were kept in room environment until their moisture content reached equilibrium condition.

NIR spectral measurement

NIR reflectance spectra were measured from the tangential face of air-dried wood samples using a Fourier transform NIR spectrophotometer (MATRIX-F, Bruker, Massachusetts; TE-InGaAs detector with a fiber optic probe with a measurement area of 7 mm^2) under laboratory conditions. A white plate (barium sulfate) served as the reference signal. To improve the signal-to-noise ratio, 32 scans were co-added at a spectral resolution of 8 cm^{-1} over the wavenumber range of 10,000–4000 cm^{-1}. A zero-filling of two (corresponding to a spectral interval of 4 cm^{-1}) was applied. Five NIR spectral measurements were made at different positions on the tangential faces and were averaged for each sample. The dimensions and weights of the samples were measured before and after the NIR spectral measurements.

Wood property measurement

After the NIR spectral measurements, static bending tests were performed. A load was applied on the tangential faces with a load cell (SL6001, Imada SS Corp., Toyohashi). The test span was set at 92.6 mm, and the load was applied at the center. The modulus of elasticity (MOE) in bending was obtained from the load–deflection curve. After the bending

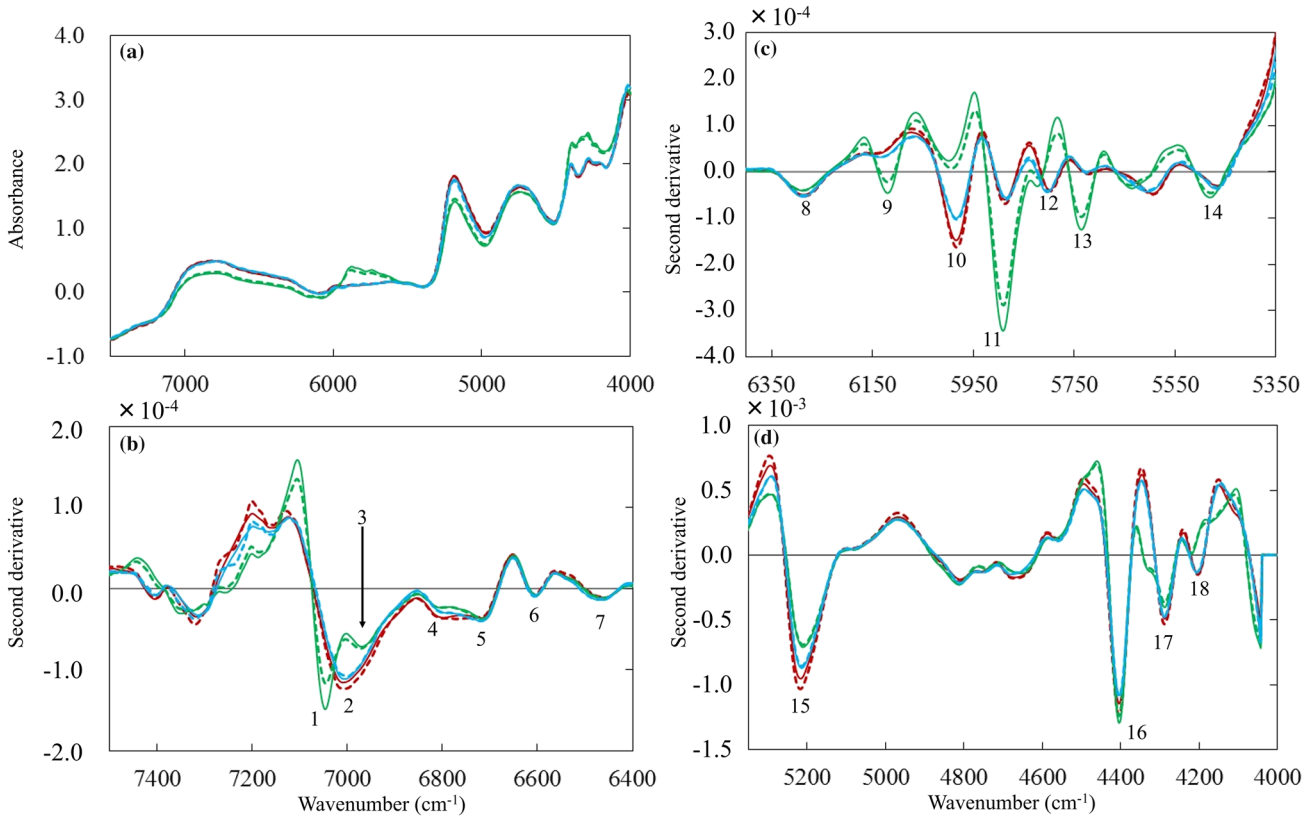

Fig. 2 NIR reflectance spectra of air-dried wood. **a** Absorption spectra at the wavenumber range of 7500–4000 cm^{-1} and second derivative spectra at the wavenumber ranges of **b** 7500–6400 cm^{-1}, **c** 6400–5350 cm^{-1}, and **d** 5350–4000 cm^{-1}. The vertical axes in **b**–**d** have different scales to clearly show the spectral features. Green solid line (NNTY99p, AD 303), green dashed line (NNTY99p, AD 253), red solid line (NNTY 59a, AD 349), red dashed line (NNTY 59a, AD 411), blue solid line (Modern, AD 1778), and blue dashed line (Modern, AD 1859)

Table 1 Assignments of near-infrared (NIR) second derivative spectra of wood

	Wavenumber (cm^{-1})	Assignment	Component	Wavenumber from reference [23] (cm^{-1})
1	7040	Not assigned		
2	7020–6998	1st OT O–H str. + H_2O	Amorphous regions in cell., water	7003–6993
3	6930	1st OT O–H str.	Lignin	
4	6795	1st OT O–H str.	Semi crystalline region in cell.	6790
5	6720	1st OT O–H str.	Semi crystalline region in cell.	6740–3700
		1st OT O–H str.	Intramolecular H-bond in cell.	≈6715
6	6595	Not assigned		
7	6450	1st OT O–H str.	Crystalline regions in C_I, O(3)-H(3)…O(5) intrachain H-bond, crystalline cell.	6460
		1st OT O–H str.	Crystalline regions in C_I, O(3)-H(3)…O(5) intrachain H-bond, crystalline cell.	6334
8	6290	1st OT O–H str.	Crystalline cell. II	6307–6267
			Strong O(2)-H(2)…O(6) of cell.	6300–6295
			Crystalline region in cell.	6281
9	6120	Not assigned		
10	6012–5980	1st OT O–H str.	Hemi.	6003
		1st OT C_{arm}–H str.	Lig.	5980, 5974, 5963, 5978
11	5902–5885	1st OT O–H str.	–	5900
		1st OT C–H str.	Lig.	5890
		1st OT C–H str.	Cell.	5872
		1st OT O–H str.	Hemi.	5865
12	5807 – 5803	1st OT O–H str.	Lig./hemi./cell.	5814, 5816
			Hemi.	5800
			Lig.	5795
13	5738	Not assigned		
14	5475	O–H str. + 2nd OT C–O	Cell.	5495
		O–H str. + 2nd OT C–O	Semi crystalline or crystalline region in cell.	5464
15	5228–5215	2nd OT C = O str.	Hemi.	5245, 5236
		O–H asym. str. + O–H def. of water	Water	5220–5150
16	4414–4402	O–H str. + C–O str.	Lig.	4411
		O-–H str. + C–O str.	Cell.	4405
		C–H_2 str. + C–H_2 def.	Cell./hemi.	4404
		C–H str. + C–H def.	Hemi.	4401
		O–H str. + C–C str. And/or C–H str. +C–H def.	Cell.	4392
17	4287	C–H str. + C–H def.	Hemi.	4296–4288
		C–H str. + C–H def.	Cell./hemi.	4283 4281
		C–H str. + C–H_2 def.	Lig.	4280
		C–H str. + C–H_2 def.	Cell.	4277
18	4208–4200	2nd OT O–H def.	Holo.	4202
		Not assigned	Lig.	4195

OT overtone, *asym*. asymmetric, *str*. stretching vibration, *bend* bending vibration, *def*. deformation vibration
Lig. lignin, *Holo*. holocellulose, *Hemi*. hemicellulose, *Cell*. cellulose

test, the wood samples were left for more than a month in a desiccator with phosphorus pentoxide to ensure that the samples reached a complete dry condition. The oven-dried wood samples were removed after equilibrium was reached, and their NIR spectra, dimensions, and weights were measured. Densities and moisture contents of the air-dried wood

samples were calculated from the physical dimensions and averaged mass of the air- and oven-dried samples. Thin tangential sections measuring approximately 50–100 µm were then sliced from sample blocks using a sliding microtome. The thin, oven-dried samples were extracted using benzene–ethanol (2:1 volume ratio) in a Soxhlet apparatus for 6 h and were then delignified for 4 h using the acid chlorite method. Extractive-free, lignin-free holocellulose was treated with sodium hydroxide and acetic acid, and the obtained residue was defined as α-cellulose.

PLS regression analysis

Wood properties (moisture content, air-dry density, air-dry MOE, extractive content, holocellulose content in wood and extractive-free wood, α-cellulose content in wood and extractive-free wood) were estimated from the NIR spectra of air-dried wood samples using PLS regression (PLS-R) analysis. OPUS Quant 2 software (Bruker, Karlsruhe, Germany) was used for data preprocessing and for calibrating and validating the PLS-R models. The spectra were processed using a 17-point smoothing filter and a second-order polynomial to obtain first derivatives, second derivatives, straight-line subtraction, min–max normalization, constant offset elimination, standard normal variate, and multiplicative scatter correction; their combination was applied to wavenumber regions for calculating the PLS-R models. The optimum number of PLS components was determined using leave-one-out full cross validation. Calibration and cross validation were evaluated based on the coefficient of determination (R^2) between predicted and measured values and root mean square error of cross validation (RMSECV), respectively. No outlier was excluded from this study. The residual prediction deviation or ratio of performance to deviation (RPD) was calculated as the ratio of two standard deviations: the standard deviation of the reference data for the validation set and the standard error of prediction from cross validation.

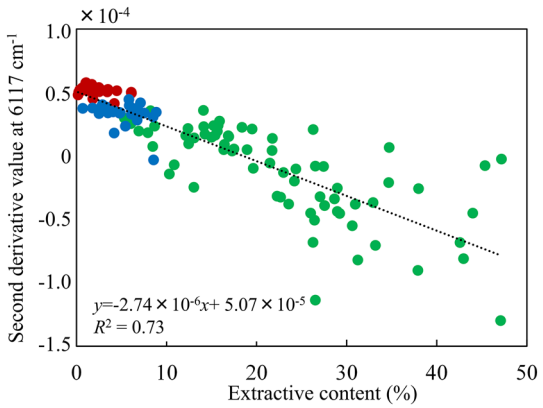

Fig. 3 Relation between NIR second derivative values at 6117 cm^{-1} and extractive contents (%). Green closed circles indicate NNTY99p wood samples, red closed circles indicate NNTY59a wood samples, and blue closed circles indicate Modern wood samples

Results and discussion

Second derivative NIR spectral change between logs

Figure 2 shows the representative NIR absorption spectra of air-dried wood samples from each log at the wavenumber range of (1) 7500–4000 cm^{-1} and the second derivative spectra at the wavenumber ranges of (2) 7500–6400 cm^{-1}, (3) 6400–5350 cm^{-1}, and (4) 5350–4000 cm^{-1}. The absorption band characteristics of the wood samples are labeled, and their assignments are summarized in Table 1. The assignments in Table 1 refer to data reported by Schwanninger et al. [27].

Table 2 Summary of second derivative spectral changes with degradation of softwood

Refs.	Fig.	Species	Degradation	6130 cm^{-1} Peak 9	5986 cm^{-1} Peak 10	5890 cm^{-1} Peak 11	5800 cm^{-1} Peak 12	5750 cm^{-1} Peak 13
	2-c	Cypress (*Chamaecyparis obtusa*)	NNTY9p	+	−	+	−	+
	2-c	Cypress (*Chamaecyparis obtusa*)	NNTY59a	−	+	NA	−	NA
17	1-a	Cedar (*Cryptomeria japonica*)	Thermal (air-dry)	NA[a]	−	−	−	NA
16	2-c	Cypress (*Chamaecyparis obtusa*)	Hygrothermal	+	NA	+	−	+
7	2-a	Cypress (*Chamaecyparis obtusa*)	Aging (Todaiji)	NA	–	+	−	NA
12	1-e	Spruce (*Picea abies* L. Karst)	White-rot fungi	NA	−	−	−	NA
12	1-e	Spruce (*Picea abies* L. Karst)	Brown-rot fungi	NA	+	−	−	NA
4	4	Pine	Waterlogged	NA	+	+	+	NA
20	4	Cypress (*Chamaecyparis obtusa*)	UV lightning	NA	−	NA	−	NA

[a]NA indicates that the spectral change with degradation was unclear

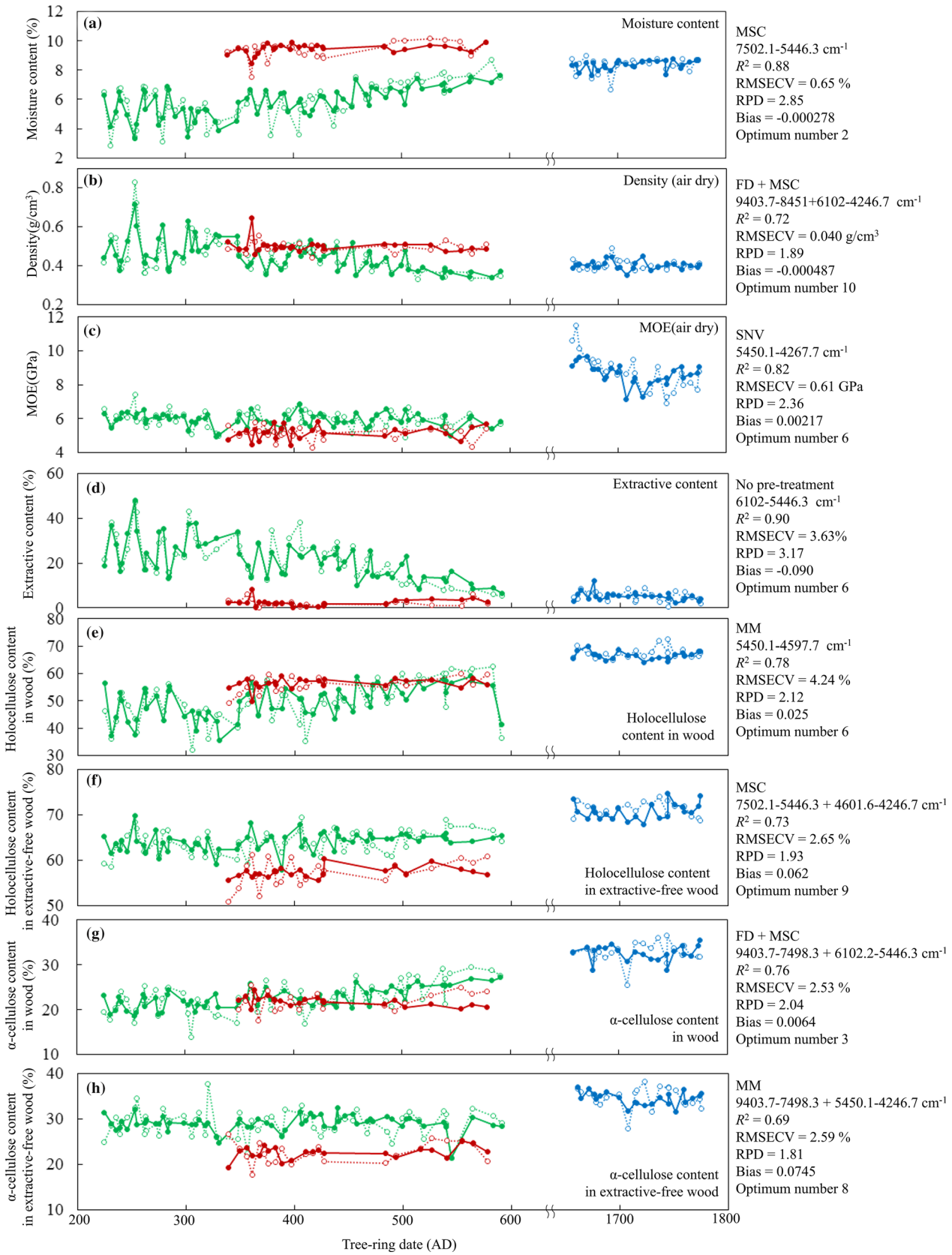
(a)
Moisture content
Moisture content (%)
MSC
7502.1-5446.3 cm-1
R2 = 0.88
RMSECV = 0.65 %
RPD = 2.85
Bias = -0.000278
Optimum number 2
(b)
Density (air dry)
Density(g/cm3)
FD + MSC
9403.7-8451+6102-4246.7 cm-1
R2 = 0.72
RMSECV = 0.040 g/cm3
RPD = 1.89
Bias = -0.000487
Optimum number 10
(c)
MOE(air dry)
MOE(GPa)
SNV
5450.1-4267.7 cm-1
R2 = 0.82
RMSECV = 0.61 GPa
RPD = 2.36
Bias = 0.00217
Optimum number 6
(d)
Extractive content
Extractive content (%)
No pre-treatment
6102-5446.3 cm-1
R2 = 0.90
RMSECV = 3.63%
RPD = 3.17
Bias = -0.090
Optimum number 6
(e)
Holocellulose content in wood
Holocellulose content in wood (%)
MM
5450.1-4597.7 cm-1
R2 = 0.78
RMSECV = 4.24 %
RPD = 2.12
Bias = 0.025
Optimum number 6
(f)
Holocellulose content in extractive-free wood
Holocellulose content in extractive-free wood (%)
MSC
7502.1-5446.3 + 4601.6-4246.7 cm-1
R2 = 0.73
RMSECV = 2.65 %
RPD = 1.93
Bias = 0.062
Optimum number 9
(g)
α-cellulose content in wood
α-cellulose content in wood (%)
FD + MSC
9403.7-7498.3 + 6102.2-5446.3 cm-1
R2 = 0.76
RMSECV = 2.53 %
RPD = 2.04
Bias = 0.0064
Optimum number 3
(h)
α-cellulose content in extractive-free wood
α-cellulose content in extractive-free wood (%)
MM
9403.7-7498.3 + 5450.1-4246.7 cm-1
R2 = 0.69
RMSECV = 2.59 %
RPD = 1.81
Bias = 0.0745
Optimum number 8
200
300
400
500
600
1700
1800
Tree-ring date (AD)

◂**Fig. 4** NIR predicted (solid line with closed circle) and measured (dashed line with open circle) wood properties as a function of the dendrochronological age. Spectral pretreatment, wavenumber used for regression, R^2, RMSECV, RPD, regression line bias, and optimum number of PLS components yielding the best R^2 are shown on the right side of each figure. MM: min–max normalization, FD: first derivative, MSC: multiplicative scattering correction, and SNV: standard normal variate

The type of degradation in wood samples that have been degraded for a long time can be estimated by comparing the second derivative spectra with the spectra acquired from other reports on the investigation of the NIR spectral change in wood caused by thermal treatment, aging in water or atmosphere, lightening, or fungal treatment. The spectral range of 6400–5400 cm^{-1} is sensitive for quantifying degradation as the effect of moisture content on these regions is insignificant. The second derivative spectral change with degradation of softwood reported in the literature has been summarized in Table 2. Because of the peak intensity and position in the second derivative spectral change with the measurement (i.e., spectral resolution and step) and pretreatment (i.e., gap, segments, and method) conditions, it is possible to understand wood degradation by observing the relative increase and decrease between the peaks.

The second derivative spectra of NNTY99p wood samples (green line) showed a different trend than that of NNTY59a (red line) and Modern (blue line) wood samples, as shown in Fig. 2b–d. The second derivative spectral change in NNTY99p wood samples is similar to that with hygro-thermal treatment reported by Inagaki et al. [16]. The relative increase in peak 3 in Fig. 2b, the increase in peak 9 with peak shift toward lower wavenumber, the increase in peak 11 with peak shift toward lower wavenumber, and the increase in peak 13 and the decrease in peak 12 in Fig. 2c compared with Modern wood were also observed for the second derivative spectra of hygro-thermally treated cypress, as shown in Fig. 2c, based on the report by Inagaki et al. [16]. Thus, we assumed that NNTY99p wood samples were in high-humidity or water-rich conditions for a long time. Although we compared the second derivative spectral change in NNTY99p wood samples with the second derivative spectra of thermally treated sugi wood in air-dry conditions [17] and of spruce treated by white- or brown-rot fungi [12] or lightening [20], the specific behavior, i.e., increase in peaks 9 and 11, was found only in hygro-thermally treated cypress [16].

The shape of the second derivative spectra of NNTY59a wood samples was similar to that of Modern wood samples despite the fact that the range of dendrochronological age was similar to that of NNTY99p wood samples. The increase at peak 10 can be clearly observed for NNTY59a compared with Modern wood samples. This behavior was also found for the second derivative spectra of spruce treated with brown-rot fungi (*Coniophora puteana*), as reported by Fackler et al. [12]. This change was attributed to the relative increase in lignin content. As the relative increase in peak 10 with degradation and the decrease in peak 12 with peak shift to a lower wavenumber can be found only in wood treated with brown-rot fungi in previous studies, we estimated that the NNTY59a wood had been degraded by brown-rot fungi with relatively minor degradation due to aging.

It is well known that most of the extractives disappear or degrade during thermal treatment; particularly, the most volatile but new compounds that can be extracted from wood appear, resulting from the degradation of cell wall structural components [28]. Figure 3 shows the relation between the second derivative values at peak 9 and the measured extractive contents. The measured extractive content in NNTY59a wood samples was slightly lower than that in Modern wood samples, although that in NNTY99p wood samples was in the range of 5–50%. Peak 9 at approximately 6130 cm^{-1} has not been assigned [27]. As the second derivative values, which correspond to the concentration of assigned functional group, at peak 9 showed a high correlation with extractive content with determination coefficient value of 0.73 as shown in Fig. 3, this peak may be assigned to functional groups in extractives resulting from the degradation of cell wall structural components. The noticeable decrease in peak 10 (mainly assigned to first overtone of OH stretching vibration of an aromatic group in lignin and hemicellulose) and increase in peak 11 (mainly assigned to first overtone of C–H stretching vibration in lignin) observed for NNTY99p (Fig. 2c) wood samples is suspected to be due to the decomposition of hemicellulose into extractives and structural changes in lignin, consistent with the results reported by Nuopponen et al. [29] in their study investigating the FT-IR spectroscopy of Scots pine planks, which were heat-treated with steam at a temperature range of 100 °C–240 °C.

From the observation of the second derivative spectra of archeological wood samples, we could estimate that NNTY59a had been dominantly degraded by brown-rot fungi, with relatively minor degradation due to aging, resulting in the degradation of extractives and hemicellulose. This spectral change in NNTY59a wood samples is consistent with the findings of Karppanen et al. [30] who reported that brown-rot fungus radically changed the extractive concentrations of Scots pine heartwood, as shown by the decrease in the concentrations of stilbenes, resin acids, and free fatty acids. On the contrary, we estimated that NNTY99p had been exposed to high-humidity or water-rich conditions, resulting in the dominant degradation of hemicellulose and cellulose into extractives. As it is not possible to completely understand the history of these archaeological wood samples, there is the possibility that these archaeological samples have been exposed to other kinds of degradation, i.e., lightning, chemical substance intrusion into wood from the

environmental. However, we can still conclude that the dominant change in the second derivative spectra of NNTY59a and NNTY99p are similar to the spectral change due to brown-rot fungi degradation and hygro-thermal treatment.

PLS prediction of the archeological wood properties

NIR spectra predicted for cross validation (solid line with closed circle) and measured wood properties (dashed line with open circle) as a function of dendrochronological age are shown in Fig. 4 (Green indicates NNTY99p, red indicates NNTY59a, and blue indicates Modern wood samples). Spectral pretreatment, regression wavenumber, R^2, RMSECV, RPD, regression line bias, and optimum number of PLS components yielding the best R^2 are shown on the right side of each figure. For all wood properties, NIR can trace the changes that occur in wood with aging.

PLS analysis provided good regression models for moisture content of wood, with $R^2 = 0.88$ (Fig. 4a). Although it the equilibrium moisture content decreases with aging or thermal treatment [1, 28], moisture content showed higher value in NNTY59a wood samples than in Modern wood samples. The NIR second derivative peaks 2 and 15 shown in Fig. 2b, d assigned to water for air-dried NNTY59a wood samples also increased compared with those of Modern wood samples, which correspond to the higher moisture content. Karppanen et al. [30] also reported that water adsorption capacity of the fungus-decayed heartwood in Scots pine is significantly higher than that of undecayed heartwood. The air-dry density of both archeological woods (Fig. 4b) was higher than that of Modern wood. We confirmed that the measured oven-dry density of NNTY99p and NNTY59a wood samples, which can also be well predicted from the NIR spectra, was higher than that of the Modern wood sample. Although the density of the archeological wood samples was higher than that of the Modern wood sample, their air-dry MOE, which was well predicted from the NIR spectra with $R^2 = 0.82$, was smaller than that of Modern wood samples (Fig. 4c). This decrease might be due to decomposition of chemical component (cellulose crystalline region), i.e., smaller amount of α-cellulose content in archaeological wood sample compared to Modern wood samples were observed as shown in Fig. 4g, h). The determination coefficients for the chemical components were $R^2 = 0.90$, 0.78, 0.73, 0.76, and 0.69 for extractive content, holocellulose content in wood, holocellulose in extractive-free wood, α-cellulose content in wood, and α-cellulose content in extractive-free wood, respectively. The extractive content in NNTY59a wood samples was in the range of 5–50%, which was slightly lower than that in Modern wood samples. Holocellulose content and α-cellulose in extractive-free wood of NNTY59a were the lowest among the three types of wood log samples, corresponding to the lowest MOE for

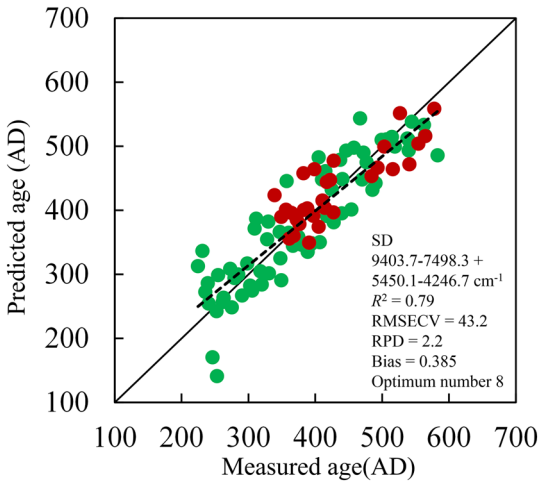

Fig. 5 Relation between the dendrochronological and NIR predicted ages. Green closed circles indicate NNTY99p wood samples, and red closed circles indicate NNTY59a wood samples. SD indicates second derivative

NNTY59a. This study showed that the physical and chemical properties of archeological wood samples can be traced using NIR spectroscopy. The changes in these properties between and within the wood samples can be well predicted as a function of distance in the radial direction.

PLS regression was constructed for determining the dendrochronological ages of NNTY59a and NNTY99p. For cross validation, high coefficients of determination between predicted and measured values were obtained with $R^2 = 0.79$ and RMSECV = 43.2 years. Figure 5 shows the relation between the dendrochronological and predicted ages, where the green and red closed circles represent NNTY99p and NNTY59a wood samples, respectively. Although the second derivative spectral change with age significantly differed, which was, therefore, expected to be more difficult to predict, the coefficients of determination obtained were good for age, physical and chemical properties, which means PLS regression analysis extracted any common spectral variation corresponding to wood parameters from archaeological wood samples.

Conclusion

The second derivative NIR spectra of air-dried archeological wood, the dendrochronological ages of which were also determined, showed specific behavior with aging. By comparing the second derivative NIR spectra at the wavenumber range of 6400–5200 cm^{-1}, we estimated that the main degradation in the log NNTY99p (determined dendrochronological age: AD 220) was because of long-term aging in

high-humidity or water-rich conditions, although the main degradation in the other log NNTY59a (determined dendrochronological age: AD 340) was estimated to be biodegradation by brown-rot fungi. Chemical and physical properties of Modern and archeological wood samples were well predicted from the NIR spectra. Although the second derivative spectral change significantly differed with age, the PLS provided a good prediction model for dendrochronological age with RMSECV = 43.2 years for NNTY99p and NNTY59a.

Acknowledgements The authors would like to acknowledge the financial support from JSPS (KAKENHI, No. 16K07805 and 26850111).

References

1. Fengel D (1991) Aging and fossilization of wood and its components. Wood Sci Technol 25:153–177
2. Pizzo B, Pecoraro E, Macchioni N (2013) A new method to quantitatively evaluate the chemical composition of waterlogged wood by means of attenuated total reflectance Fourier transform infrared (ATR FT-IR) measurements carried out on wet material. Appl Spectrosc 67:553–562
3. Sandak A, Sandak J, Babinski L, Pauliny D, Riggio M (2014) Spectral analysis of changes to pine and oak wood natural polymers after short-term waterlogging. Polym Degrad Stabil 99:68–79
4. Pecoraro E, Pizzo B, Alves A, Macchioni N, Rodrigues JC (2015) Measuring the chemical composition of waterlogged decayed wood by near infrared spectroscopy. Microchem J 122:176–188
5. Yonenobu H, Tsuchikawa S (2003) Near-infrared spectroscopic comparison of antique and modern wood. Appl Spectrosc 57:1451–1453
6. Arnott SHL, Dix JK, Best AI, Gregory DJ (2005) Imaging of buried archaeological materials: the reflection properties of archaeological wood. Mar Geophys Res 26:135–144
7. Tsuchikawa S, Yonenobu H, Siesler HW (2005) Near-infrared spectroscopic observation of the ageing process in archaeological wood using a deuterium exchange method. Analyst 130:379–384
8. Sandak A, Sandak J, Zborowska M, Pradzynski W (2010) Near infrared spectroscopy as a tool for archaeological wood characterization. J Archaeol Sci 37:2093–2101
9. Sandak A, Rozanska A, Sandak J, Riggio M (2015) Near infrared spectroscopic studies on coatings of 19th century wooden parquets from manor houses in South-Eastern Poland. J Cult Herit 16:508–517
10. Fackler K, Gradinger C, Hinterstoisser B, Messner K, Schwanninger M (2006) Lignin degradation by white rot fungi on spruce wood shavings during short-time solid-state fermentations monitored by near infrared spectroscopy. Enzyme Microb Tech 39:1476–1483
11. Fackler K, Schwanninger M, Gradinger C, Hinterstoisser B, Messner K (2007) Qualitative and quantitative changes of beech wood degraded by wood-rotting basidiomycetes monitored by Fourier transform infrared spectroscopic methods and multivariate data analysis. Fems Microbiol Lett 271:162–169
12. Fackler K, Schwanninger M, Gradinger C, Srebotnikl E, Hinterstoisser B, Messner K (2007) Fungal decay of spruce and beech wood assessed by near-infrared spectroscopy in combination with uni- and multivariate data analysis. Holzforschung 61:680–687
13. Fackler K, Schwanninger M (2012) How spectroscopy and microspectroscopy of degraded wood contribute to understand fungal wood decay. Appl Microbiol Biot 96:587–599
14. Fackler K, Schwanninger M (2010) Polysaccharide degradation and lignin modification during brown rot of spruce wood: a polarised Fourier transform near infrared study. J Near Infrared Spec 18:403–416
15. Fackler K, Schwanninger M (2011) Accessibility of hydroxyl groups of brown-rot degraded spruce wood to heavy water. J Near Infrared Spec 19:359–368
16. Inagaki T, Mitsui K, Tsuchikawa S (2008) Near-infrared spectroscopic investigation of the hydrothermal degradation mechanism of wood as an analogue of archaeological objects. Part I: Softwood. Appl Spectrosc 62:1209–1215
17. Inagaki T, Matsuo M, Tsuchikawa S (2016) NIR spectral–kinetic analysis for thermally degraded sugi (*Cryptomeria japonica*) wood. Appl Phys A-Mater 122:208
18. Mehrotra R, Singh P, Kandpal H (2010) Near infrared spectroscopic investigation of the thermal degradation of wood. Thermochim Acta 507–508:60–65
19. Todorovic N, Popovic Z, Milic G (2015) Estimation of quality of thermally modified beech wood with red heartwood by FT-NIR spectroscopy. Wood Sci Technol 49:527–549
20. Tsuchikawa S, Inoue K, Mitsui K (2004) Spectroscopic monitoring of wood characteristics variation by light-irradiation. Forest Prod J 54:71–76
21. Mitsui K, Tsuchikawa S (2003) Application of near infrared spectroscopy (NIR) to light-irradiated wood. Holz Roh Werkst 61:159–160
22. Matsuo M, Yokoyama M, Umemura K, Sugiyama J, Kawai S, Gril J, Kubodera S, Mitsutani T, Ozaki H, Sakamoto M, Imamura M (2011) Aging of wood: Analysis of color changes during natural aging and heat treatment. Holzforschung 65:361–368
23. Inagaki T, Asanuma Y, Tsuchikawa S (2017) Selective assessment of duplex heat-treated wood by near-infrared spectroscopy with principal component and kinetic analyses. J Wood Sci 64:6–15
24. English Heritage 2004 (1998) Dendrochronology—guidelines on producing and interpreting dendrochronological dates, p 39. https://historicengland.org.uk/images-books/publications/dendrochronology-guidelines/.. Accessed 14 Feb 2018
25. Yonenbu H, Eckstein D (2006) Reconstruction of early spring temperature for central Japan and its verification by other proxy records. Geophys Res Lett 33:L10701
26. Ohyama M, Yonenobu H, Choi JN, Park WK, Hanzawa M, Suzuki M (2013) Reconstruction of northeast Asia spring temperature. Clim Past 1784–1990:9: 261–266
27. Schwanninger M, Rodrigues JC, Fackler K (2011) A review of band assignments in near infrared spectra of wood and wood components. J Near Infrared Spec 19:287–308
28. Esteves BM, Pereira HM (2009) Wood modification by heat treatment: A review. Bioresources 4:370–404
29. Nuopponen M, Vuorinen T, Jamsa S, Viitaniemi P (2004) Thermal modifications in softwood studied by FT-IR and UV resonance Raman spectroscopies. J Wood Chem Technol 24:13–26
30. Karppanen O, Venalainen M, Harju AM, Laakso T (2008) The effect of brown-rot decay on water adsorption and chemical composition of Scots pine heartwood. Ann For Sci 65:610